Electronic structure of the Nowotny chimney-ladder silicide Ru_2Si_3

W. Wolf
Institut für Physikalische Chemie der Universität Wien, Liechtensteinstraße 22a, A-1090 Wien, Austria

G. Bihlmayer* and S. Blügel†
Institut für Festkörperforschung, Forschungszentrum Jülich, D-52425 Jülich, Germany
(Received 20 May 1996)

We report *ab initio* calculations for the electronic structure of the Nowotny chimney-ladder silicide Ru_2Si_3 in the orthorhombic low-temperature phase. We find Ru_2Si_3 to be a semiconductor with a direct band gap of about 0.45 eV. Since this gap is a p-d gap, the oscillator strength for a direct transition is expected to be of sizable magnitude. Also, the calculated effective masses of hole and electron states suggest that Ru_2Si_3 is a very promising material for various applications in semiconductor technology. The electronic structure is controlled by the hybridization of Si p states with Ru d states and shows similarities to the group-IV transition-metal disilicides ($CrSi_2$, $MoSi_2$, WSi_2) and to transition-metal-rich silicides. The calculations are based on the density-functional theory in local-density approximation and are performed by means of the full-potential linearized-augmented-plane-wave method. [S0163-1829(97)12007-0]

I. INTRODUCTION

Transition-metal silicides have been studied intensively in the last decade because of their practical importance in a silicon-based very-large-scale-integrated microelectronic device technology[1–3] as low-resistivity interconnects, gate metalizations, and Schottky barriers. The interest in silicides originates from their electronic properties in conjunction with the possibility of epitaxial growth in and on Si.

The absolute majority of silicides is known to have metallic type of conductivity,[4] and only a few silicides have been identified as semiconductors, with typical band gaps in the range of 0.1–0.9 eV.[5] These semiconducting silicides have attracted attention because of their potential application as optoelectronic devices such as light sources, infrared detectors, electro-optic interconnects, etc. that can be fully integrated with the current silicon microelectronic components.[6]

$CrSi_2$ is presumably experimentally[6,7] as well as theoretically[8–13] the most intensively studied example among the semiconducting silicides. From the measurements[7] it is reported that $CrSi_2$ exhibits an indirect band gap of about 0.35 eV, which basically was confirmed by band-structure calculations which found indirect gaps of about 0.3 eV. This band gap is derived from the hybridization of Si p states with Cr d states, and it is located in the midst of mainly Cr d states. This band gap is a generic feature of the band structures of a large variety of transition-metal (TM) disilicides $TMSi_2$: ten TM d and 2×6 Si p states per formula unit are grouped in ten p-d bonding states, separated from ten p-d antibonding states and two nonbonding p states. Many-atom interaction may rearrange the electronic structure further and in some cases the band structures exhibit a partial gap such as for $TiSi_2$ (Ref. 14) in its orthorhombic structure, or for $MoSi_2$ (Refs. 15–20) and WSi_2 (Refs. 15, 19, and 21) in their tetragonal ground-state structures. In some instances a true band gap occurs such as for $MoSi_2$,[9,13,18,19] grown as thin films[22,23] in the metastable hexagonal $CrSi_2$ structure, or the band gap just collapses as for WSi_2 (Refs. 9, 13, and 19) also stabilized in the metastable hexagonal $CrSi_2$ structure.[22,24]

On the search for further semiconducting silicides, it is worth mentioning that $CrSi_2$ has 14 valence-electrons (ve) per transition-metal atom (veTM) and the Fermi energy (E_F) is located in the band-gap separating filled valence-band states from empty conduction-band states. For $MoSi_2$ and WSi_2, which are isoelectronic to $CrSi_2$, the Fermi energy is also located in the band gaps of the hexagonal structures or in the partial gap of the tetragonal one, respectively. On the other hand, VSi_2, which crystallizes also in the $CrSi_2$ structure, has only 13 veTM, and the Fermi energy is located below the partial gap and it is a metal.[9] The same is true for $TiSi_2$,[14] which has 12 veTM.

Ruthenium sesquisilicide Ru_2Si_3 is a further silicide with 14 veTM. It is reported to be semiconducting[25,26] with a band gap of about 0.7 eV,[25] it can be grown epitaxially on Si(111) (Ref. 27) and single crystals can be made.[28] Ru_2Si_3 also exhibits interesting thermoelectric characteristics.[28] With these properties Ru_2Si_3 is a promising candidate for technological applications.

Ru_2Si_3 is a member of a large, but sparsely investigated family of transition-metal compounds, known as the defect-$TiSi_2$ compounds[29] or the stuffed white tin structures,[30] for which Pearson[31] coined the descriptive term Nowotny ''chimney-ladder'' compounds. As for the tetragonal $MoSi_2$ structure, the hexagonal $CrSi_2$ structure or the orthorhombic $TiSi_2$ structure, the building principle of the chimney-ladder compounds consists of close-packed-hexagonal (hcp) layers of TM disilicides. These hcp layers appear in the planes parallel to $MoSi_2(110)$, $CrSi_2(0001)$, or $TiSi_2(100)$, respectively. In the chimney-ladder compounds the mode of stacking is as in $TiSi_2$, e.g., the TM atoms form approximately equilateral triangular nets, which are stacked in the stacking sequence $ABCD$, arising when the TM vertex of one net does not fill the trigonal voids but the saddle point or bridge positions, respectively, between the TM atoms. These hexagonal layers are parallel to the (101) plane of the

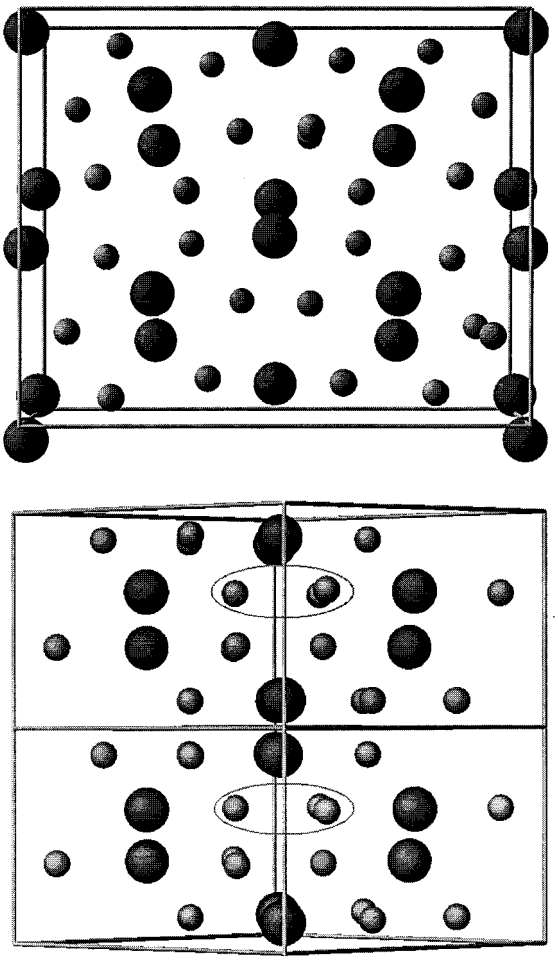

FIG. 1. The unit cell of Ru_2Si_3 (top) compared to two $TiSi_2$ unit cells seen from the [001] and [101] directions respectively. Large spheres indicate Ru (Ti) atoms, small spheres Si sites. Notice, that the Ru_2Si_3 structure corresponds to the $TiSi_2$ structure with one-fourth of the Si atoms missing (the ellipse indicates missing Si atoms).

chimney-ladder compounds and lead to a TM sublattice, which can be described by β-Sn-like pseudo-unit-cells, stacked along the [001] direction in case of the tetragonal chimney-ladder compounds or stacked in the [100] and [001] directions as in the orthorhombic compounds. With respect to the disilicides the composition of the defect-$TiSi_2$ silicides is changed by a regular expansion of the Si sublattice, while the sublattice of TM atoms remains unchanged (see Fig. 1). The composition and the number of β-Sn-like pseudo-unit-cells of transition-metal atoms of the defect-$TiSi_2$ structures is controlled by the valence-electron concentrations in such a way that the number of valence-electrons per transition metal site never exceeds the ''magic'' number of 14 veTM.[29,31,32] Due to the similarity to the above-mentioned group-VI silicides such as $CrSi_2$ (stacking sequence ABC instead of $ABCD$), it is speculated that the structures are stabilized by a 14 veTM gap between bonding and antibonding states formed by Si p and TM d electrons. Following a rigid-band model, structures with more than 14 veTM would lose their stability, since the Fermi energy lies above the gap.

For a p-d gap material the across-gap oscillator strength for dipole-allowed transitions between the top of the valence band and the bottom of the conduction band are expected to be sizable. Therefore, expectations about the optical properties of Ru_2Si_3 are rated much higher than for β-$FeSi_2$, which is a d-d gap semiconductor[33] and has a vanishingly small oscillator strength.[34]

Because of the potential of Ru_2Si_3 in future technological applications, an understanding of the bulk electronic properties is highly desirable. Previous band-structure calculations[35] based on the empirical tight-binding method indicate the existence of a band gap with a width of the same order of magnitude as found by the experiments, but the band gap was actually not found. Lacking any detailed knowledge of the electronic structure, we have carried out *ab initio* electronic band-structure calculations for the low-temperature phase of Ru_2Si_3. We find Ru_2Si_3 to be a a semiconductor with a direct band gap at the Γ point of about 0.45 eV. The character of the wave functions changes across the gap by $\Delta l=1$ from p to d states, and we expect interesting optical properties. We argue that the true band gap may be larger by a factor of 2. Although the existing experimental data on the electronic properties of Ru_2Si_3 are quite sparse, limited to electrical resistivity,[25,26] magnetic susceptibility[25] and Hall measurements,[26,28] it is anticipated that this material will be the focus of more comprehensive experimental investigations in the future.

II. CRYSTAL STRUCTURE

Ru_2Si_3 crystallizes below $\sim$1000 °C in the low-temperature phase, which is orthorhombic[36,37] with the international space group symbol $Pbcn$ (Schönflies notation: D_{2h}^{14}), the Patterson symmetry $Pmmm$ and the space group number No. 60.[38] Above $\sim$1000 °C, a first order phase transition[39] is reported from the orthorhombic phase to a tetragonal Ru_2Sn_3-type phase with the space group symbol $P4c2$ (No. 116). This phase transformation is reversible and occurs gradually over a wide temperature range, where the Si atoms are displaced from the $Pbcn$ structure and pass through the intermediate orthorhombic phase $Pb2n$ (No. 30), while the Ru atoms remain static.

The orthorhombic $Pbcn$ unit cell contains 40 atoms, 16 Ru atoms, and 24 Si atoms, which is equivalent to 16 formula units of $RuSi_2$ minus eight missing Si defect atoms. The unit cell contains three inequivalent Ru and three inequivalent Si sites denoted by Ru(1), Ru(2), Ru(3) and Si(1), Si(2), Si(3), respectively. Unless stated otherwise, the calculation is performed using the experimental lattice parameters and the experimental atomic positions taken from Poutcharovsky and Parthé,[36] which are collected in Table I. Calculations that use another, slightly different crystallographic data set given by Israiloff and Völlenkle[37] will be discussed in Sec. IV C. The unit cell and the arrangement of the individual atoms are illustrated in Fig. 1 (top). The large and small circles represent the Ru and Si atoms, respectively. The Ru atoms are arranged close to the ideal positions of atoms in four unit cells of β-Sn or as the Ti atoms in four unit cells of $TiSi_2$, where two unit cells are stacked one on top of the other, which is then doubled in the horizontal direction in Fig. 1. When the unit cell of Ru_2Si_3 is cut along the (101) plane, one finds the Ru atoms located in centered

TABLE I. Space group, Pearson symbol, and lattice parameters of Ru_2Si_3. The atomic positions (multiplicity and Wyckoff letter) and their internal parameters are given together with the core shell and the muffin-tin radii R_{MT}.

Ru_2Si_3	$Pbcn$	$oP40$				
	$a=20.895$ a.u.		$b=16.883$ a.u.		$c=10.456$ a.u.	
atom	position	x	y	z	core	R_{MT}
Ru(1)	4(c)	0	0.0451	0.25	[Kr]	2.20 a.u.
Ru(2)	4(c)	0	0.5748	0.25		
Ru(3)	8(d)	0.2472	0.1864	0.2401		
Si(1)	8(d)	0.4275	0.2841	0.4537	[Ne]	1.95 a.u.
Si(2)	8(d)	0.3253	0.4350	0.0934		
Si(3)	8(d)	0.1366	0.3994	0.3946		

rectangular squares as it is known from cutting a body centered cube along the [110] direction. These centered rectangular squares are the hexagonal building blocks common to the $TiSi_2$ structure as shown in Fig. 1 (bottom). In opposite to the $TiSi_2$ structure, which has four Si atoms in a centered rectangular square, Ru_2Si_3 contains only three Si atoms, and to accommodate for the Si defects the remaining Si atoms of the Ru_2Si_3 structure are not in the plane as in $TiSi_2$ but have moved out of the generating plane to find ideal positions between the transition-metal atoms.

The structure can also be described in terms of Si polyhedra which build the RuSi coordination polyhedra.[38] We find two deformed $RuSi_4$ tetrahedra atom-type Ru(2), four $RuSi_7$ polyhedra around atom type Ru(3), and two $RuSi_6$ octahedra around atom-type Ru(1). The average interatomic Ru-Si distance varies only by about 5% from tetrahedra with 4.460 a.u. and octahedra with 4.498 a.u. to 4.668 a.u. for the $RuSi_7$ polyhedra. The variation within the polyhedra is largest for $RuSi_7$ with about 10%. Each Ru atom has four Ru neighbors. Each Si atom has four Ru neighbors with an average Ru-Si distance of 4.573, 4.639, and 4.573 a.u. for Si(1), Si(2), and Si(3) sites. Ru_2Si_3 in the $Pbcn$ phase has similar Ru-Si and Si-Si nearest neighbor distances of about 4.5 and 5.0 a.u., respectively, without any particularly short Ru-Ru (5.7 a.u.) bond length.

III. CALCULATIONAL METHOD

The calculations are based on the density-functional theory (DFT) in the local-density approximation (LDA). For the exchange and correlation potential, we used the Hedin-Lundqvist parametrization.[40] The density-functional equations are solved by applying the full-potential linearized-augmented-plane-wave (FLAPW) method,[41] which is known to be precise for transition metals with localized d wave functions in open crystal structures. The eigenstates of the core electrons (Ru: [Kr], Si: [Ne]) are obtained as solutions of the Dirac equation, and for the valence-electrons we used a scalar-relativistic approach. The formation of the gap was monitored with respect to the two most important cutoff parameters inherent in the FLAPW method: the number of basis functions to expand the wave functions and the number of **k** points to perform the Brillouin-zone integration of the charge density. We performed self-consistent calculations with 55 and 75 linearized augmented plane waves (LAPW) per atom as variational basis sets and 9, 15 and 30 **k** points have been used in the irreducible wedge (IBZ) of the primitive orthorhombic Brillouin zone (see Fig. 2) of Ru_2Si_3, which forms one-eighth of the entire Brillouin zone. We utilized the linear tetrahedron method[42] for the Brillouin-zone integration. We found that the electronic structure was well converged with 75 LAPW's and 15 **k** points. The effective-mass tensor of electrons and holes, which depends on the curvature of the band structure, turned out to be the most critical quantity with respect to the number of plane waves. Reliable results were obtained with 100 LAPW's per atom as was confirmed by calculations with 140 basis functions taken into account. The corresponding cutoff for the Fourier-series expansion of the interstitial charge density and potential was chosen to include about 32 000 plane waves. The muffin-tin radii R_{MT} of the different types of Si and Ru were chosen to be $R_{MT}(Si)=1.95$ a.u. and $R_{MT}(Ru)=2.20$ a.u., and the charge, potential, and wave functions within the sphere are represented on a radial mesh with 361 grid points with a logarithmic increment of 0.03. The LAPW wave functions within the MT's have been expanded in spherical harmonics with angular momenta through $l=6$. The linearization energies, for which the radial basis functions are solved, are positioned in the center of the l-projected and atom-type-projected occupied states. The nonspherical contributions to the charge density and potential within the MT's are expanded in lattice harmonics, which include all terms with $l\leqslant 6$. The band structure was plotted with 245 **k** points along the high-symmetry lines, and the density of states (DOS) was plotted using 90 **k** points in the IBZ.

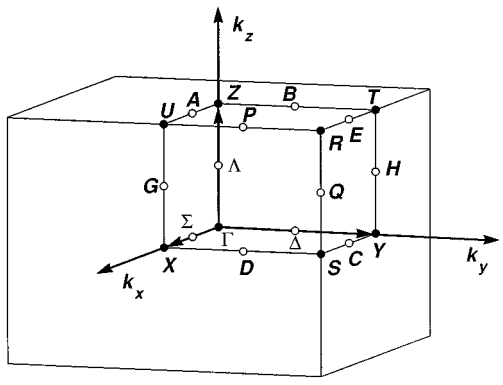

FIG. 2. Brillouin zone for the primitive orthorhombic structure $Pbcn$. The high symmetry points are chosen according to Bradley and Cracknell (Ref. 47).

IV. RESULTS AND DISCUSSION

A. Band structure

The FLAPW energy-band structure results for the low-temperature $Pbcn$ phase of Ru_2Si_3 are shown in Figs. 3 and 4. With eight formula units of Ru_2Si_3 per orthorhombic unit cell, which contains 224 valence electrons, that arise from 16 Ru $5s$ states, 112 Ru $4d$ states, 48 Si $3s$ states and 48 Si $3p$ states in the atomic configuration, a very complicated valence-conduction energy-band structure evolves. The 112 valence and some 48 conduction bands that are shown in the figures span an energy range of about 18 eV. Because of the low (D_{2h}) point symmetry of Ru_2Si_3, the energy-band states are, in general, singly degenerate throughout most of the Brillouin zone. Exceptions arise for states with wave vectors in the Brillouin-zone faces, where a twofold degeneracy is induced by the nonsymmorphic nature of the D_{2h}^{14} space group.[44] Such degeneracies occur along the high-symmetry lines Y-S-R-T and Z-U-X denoted in Fig. 2.

Despite this complexity, in Fig. 3 we can easily distinguish three energy regions: (i) the filled low-lying bands between 7 and 12 eV below the Fermi energy (E_F=0 eV). These bands show a broad, partially parabolic dispersion of nearly free-electron-like bands, and as shown below, are identified as bonding states formed predominantly by the Si-Si $3s$-$3s$ hybridization and the hybridization of Si $3s$ states with Ru $4d$ states. These bands are separated by a small band gap of about 0.1 eV from the second group of states (ii), which occupy a broad energy region, and are identified below as the Si-Ru p-d hybridization region, starting about 6 eV below the Fermi energy and reaching up to E_F. These bands are dominated by Ru $4d$ states, but contain

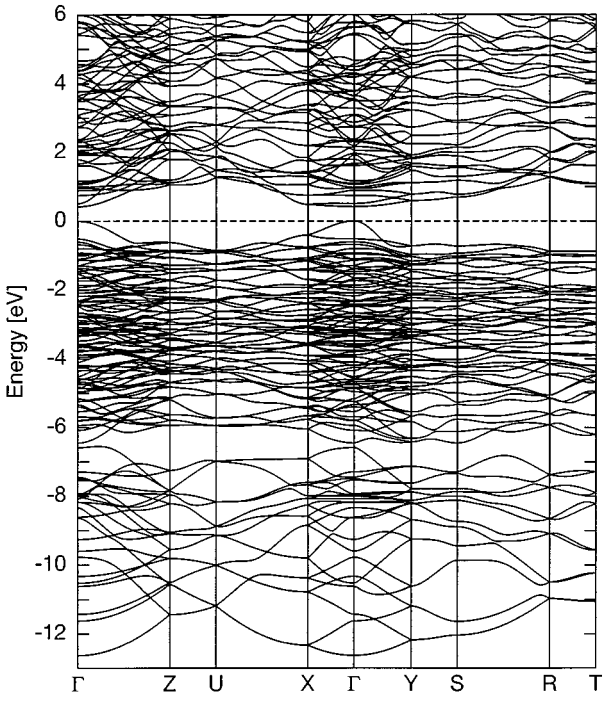

FIG. 3. Band structure of Ru_2Si_3 along symmetry lines in the first Brillouin zone. The position of the Fermi energy (E_F) is indicated by a horizontal dashed line at E=0 eV. The notation of the high-symmetry points was chosen according to Bradley and Cracknell (Ref. 47), and are indicated in Fig. 2.

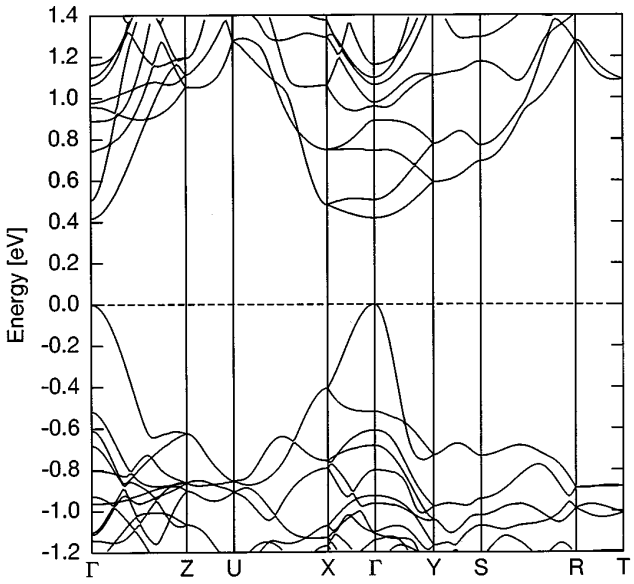

FIG. 4. Band structure of Ru_2Si_3 in the vicinity of the Fermi energy.

important contributions from Si $3p$ states. The dispersion is rather flat as it is known for states involving d electrons. Above the gap we find a third group of Ru $4d$–Si $3p$ states (iii) with somewhat larger dispersion. As discussed above, the formation of covalent Ru $4d$–Si $3p$ bonds is crucial for the stability and formation of this structure. Accordingly, we find a band-gap-controlled energy region in the middle of this p-d band complex [separating (ii) and (iii)]. The Fermi energy, which is positioned in the middle of this gap-type energy region, separates the filled valence-band states $E_{n\mathbf{k}}$ with $n \leqslant 112$ from the empty conduction-band states $E_{n\mathbf{k}}$ with $n \geqslant 113$. The dispersion of the valence-band states is flatter than those of the conduction-band states, indicative of a stronger emphasis of Si p states in the conduction-band region.

In the band-structure plot zoomed in the vicinity of the gap (Fig. 4), we find a single band (n=112) of high dispersion reaching up to the Fermi energy at the Γ point, approximately 0.4 eV higher than the next-lowest-lying band. The approximate l character of four states $E_{n\mathbf{k}}$ encompassing the energy gap at the high-symmetry points $\mathbf{k}=\Gamma$, $\mathbf{k}=X$, and $\mathbf{k}=Z$ are listed in Table II. We see that these states are predominantly formed by Ru d and Si p electrons with some contributions from Ru p and Si s electrons. The topmost state of the valence band is of high (25%) Si p character mixed with 10% Ru d and smaller contributions of Ru p- and Si s-like charge. It is interesting to note that both atoms, the Si(2) that contributes most of the p character to the valence and Ru(3) that accounts for 58% of the conduction state lie neatly grouped around the $(\frac{1}{4}\,00)$ and $(\frac{3}{4}\,00)$ plane of the unit cell. The highest valence band at point Γ (and also, to a lesser extent at X and Z) is somewhat exceptional in that it has almost 50% of its charge in the interstitial region.

At the X and Z points, the states n=111 and 112 are degenerate, and form the top of the valence bands, and the states n=113 and 114 are degenerate and form the bottom of the conduction bands. At X, the situation is quite similar to the situation at the Γ point. The top valence band has less Si

TABLE II. Partial charges (% of charge inside the corresponding muffin-tin sphere) of the states around the gap at the Γ, *X*, and *Z* points. The energies are given relative to the Fermi energy E_F. The three different rows of data per band give results for the three inequivalent Ru and Si atoms as were listed in Table I.

State	Band no.	Energy (eV)	Ru *s*	Ru *p*	Ru *d*	Si *s*	Si *p*	Si *d*
Γ	111	−0.518	0.1	0.8	8.9	2.4	4.4	0.5
			0.1	2.5	20.9	0.0	2.5	0.6
			0.1	2.2	5.7	0.6	8.0	0.3
	112	0.0	0.3	1.2	1.7	2.2	5.0	1.0
			0.0	2.9	4.9	0.0	12.8	0.6
			0.2	3.4	3.5	3.1	7.3	0.8
		gap						
	113	0.418	0.3	0.0	4.1	0.0	0.8	0.0
			0.6	0.0	6.0	0.3	3.9	0.6
			1.3	0.2	57.9	0.0	2.5	0.5
	114	0.507	0.0	0.2	1.3	0.1	1.4	0.3
			0.0	0.3	1.3	0.2	7.9	0.8
			3.8	0.4	45.7	0.0	5.1	0.6
X	111/112	−0.406	0.3	1.1	4.3	3.9	4.8	0.8
			0.0	3.5	8.9	0.1	5.9	0.5
			0.5	1.8	7.7	2.5	8.0	0.5
		gap						
	113/114	0.483	0.1	0.2	1.9	0.0	1.1	0.1
			0.3	0.3	3.8	0.3	6.3	0.7
			2.1	0.3	50.5	0.2	4.4	0.5
Z	111/112	−0.624	0.0	0.7	18.0	1.2	1.3	0.6
			0.0	0.6	12.7	0.4	1.9	0.7
			0.0	1.4	33.2	0.3	1.9	0.8
		gap						
	113/114	1.054	0.1	0.4	10.2	3.0	1.9	0.2
			0.2	0.2	20.9	1.4	1.3	0.6
			0.0	0.3	36.4	0.2	1.9	0.3

p character but still most of the charge is in the interstitial region. The Ru *d* character has doubled as compared to Γ and the Ru *p* and Si *s* contributions are nearly the same (approximately 6%). The conduction band is almost unchanged. Going to the *Z* point the charge distribution changes, and we have dominantly Ru *d* character in the electron and hole states, and the same also applies for most of the other states of lower energy.

B. Density of states

A comprehensive overview of the electronic structure is provided by the DOS results shown in Figs. 5 and 6. The DOS's shown in Fig. 5 have been averaged over the three inequivalent Ru and Si atom types. The top panel of Fig. 5 exhibits clearly the narrow gap at −7 eV and the band gap at E_F. More detailed information is provided by Fig. 6, where the DOS is decomposed for the three inequivalent Si and Ru atoms (LDOS), and is further decomposed into the different angular momentum contributions (LPDOS) for *s*-, *p*-, and *d*-like charges. We find that the inequivalent sites lead to rather similar LPDOS's. Larger deviations are found for the Si *s* states in the first energy regime, for the Ru *d* states between −6 eV and E_F, and at the bottom of the conduction bands.

The dominating feature in the DOS of Ru_2Si_3 arises between about −6 and about −1 eV from the direct Ru-Ru $4d$-$4d$ overlap (first panel in Fig. 6) forming *d*-*d* bonding and antibonding states. Compared to the *d*-band-width of about 8 eV for the plain hexagonal Ru metal, the *d*-band-width of Ru_2Si_3 is decreased. The reduction of the Ru-Ru hybridization accounts for this decrease in the *d*-band-width. For the silicide the number of nearest-neighbor Ru-Ru bonds is reduced from 12 to 4. If we assume the tight-binding limit where the *d*-band-width is proportional to the square root $\sqrt{N}$ of the number of nearest-neighbor atoms *N*, the band-width of the Ru $4d$ bands reduces by $\sqrt{\frac{4}{12}}=0.6$. Further reduction of the bandwidth of more than 30% comes from the large increase of the interatomic Ru-Ru distance (5.7 a.u.) as compared to the pure metal (5.0 a.u.). Adding up all the factors it is surprising, that the *d*-band-width is still that large.

The Ru $4d$ states are broadened by the hybridization with the Si $3p$ states (fifth panel in Fig. 6) and to much less extent with the Ru $5p$ states, which are both spread over an energy region starting at −6 eV and ending above 5 eV. Two interesting characteristics of the Si *p* LPDOS can be observed: (i) the close match between the Ru *d* states and the Si *p* states

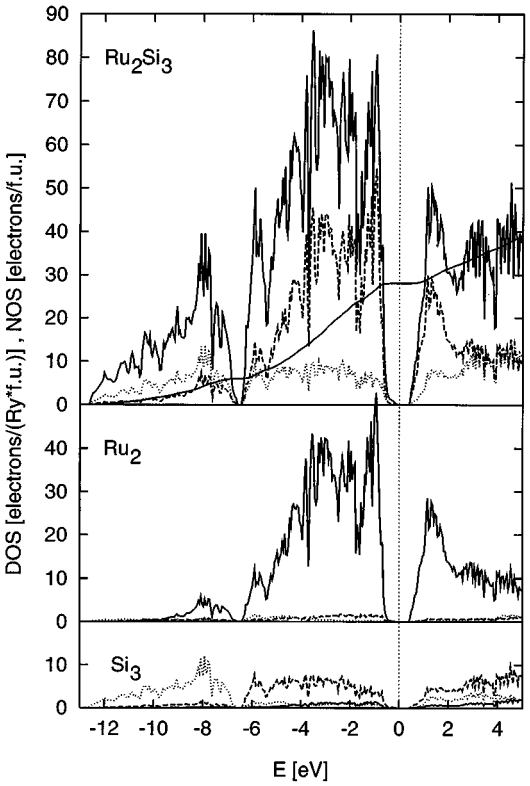

FIG. 5. Density-of-states (DOS) of Ru_2Si_3. Top panel shows the total DOS (full line) decomposed into the local, muffin-tin projected (L)DOS of Ru_2 (long dashed line) and Si_3 (short dashed line). The middle and bottom panel show the LDOS of Ru_2 and Si_3, respectively, decomposed into angular momentum contributions *s* (short dashed line), *p* (long dashed line) and *d* (full line). For Ru the *s* and *p* DOS are insignificant compared to *d* contributions. The top panel contains also the number-of-states (NOS) (full line, same scale). DOS and NOS are expressed in units of electrons/Rydberg per formula unit (f.u.) and electrons/f.u., respectively. The DOS is averaged over the three different Ru and Si sites. Fermi energy is indicated by a vertical dotted line at $E=0$ eV.

especially at the extremities of this energy region, and (ii) a parabolic reduction of the LPDOS which is located symmetrically around the gap. Both suggest the crucial role of the Si-Ru *p*-*d* hybridization. If we assume a square-root-like Si *p* LPDOS which is due to hypothetical Si atoms, which do not hybridize with the Ru atoms, and if we assume at the same time hypothetical Ru-Ru *d*-*d* hybrids, which do not hybridize with the Si atoms, then the hybridization of this Si *p* electrons with the hypothetical Ru-Ru *d*-*d* hybrids will form Si-Ru *p*-*d* hybrids, which will covalently split around the center of the Ru *d* bands. This is the origin for the parabolic reduction of the Si *p* LPDOS with a minimum around the center of the Ru *d* bands and with the main weight at the edges of the above-mentioned energy region. At the same time it is the origin of the rather asymmetrical shape of the Ru *d* states, which is due to *p*-*d* hybrids hybridized above the Fermi energy. The fact, that the states above E_F have a significant and mostly dominating Si *p* character, explains the earlier observation, that the band dispersions above E_F are larger than below E_F, where the Ru *d* electrons are the dominating states. The shape of the Si *p* LPDOS depends on the strength of the Ru-Si hybridization and the parabolic shape is common for the TM-rich silicides rather than for the TM disilicides.

The most important feature of the DOS of Ru_2Si_3 is the gap at E_F, which has been identified already for the TM disilicides as being due to the separation of the covalently formed *p*-*d* bonding states from the *p*-*d* antibonding states and nonbonding *p* states, except that we are dealing here with 38 *p* and *d* states per formular unit as compared to 22 for the TM disilicides. The states in the immediate vicinity of the gap are Ru *d*, Si *p*, and a small contribution of Ru *p* states at the valence-band edge. The strength of the hybridization between the TM *d* electrons with the Si *p* electrons[20] plays an important role for the formation of the gap. For example transition-metal-rich compounds, for which the absolute *p*-*d* hybridization is weakened, usually lose their gap.[20] This and the fact that the gap in Ru_2Si_3 is situated already at the end of the basic Ru-Ru *d*-*d* bands might be reasons why a Rh_4Si_5 Nowotny chimney-ladder silicide with 14 veTM was never reported.

The states which are split off from the *p*-*d* hybridization region below 7 eV of E_F exhibit an overall square-root increase starting from the valence-band edge at about -12 eV. They consist of about one-third Ru *d* electrons (middle panel of Fig. 5) and about two-third Si *s* electrons (bottom panel).

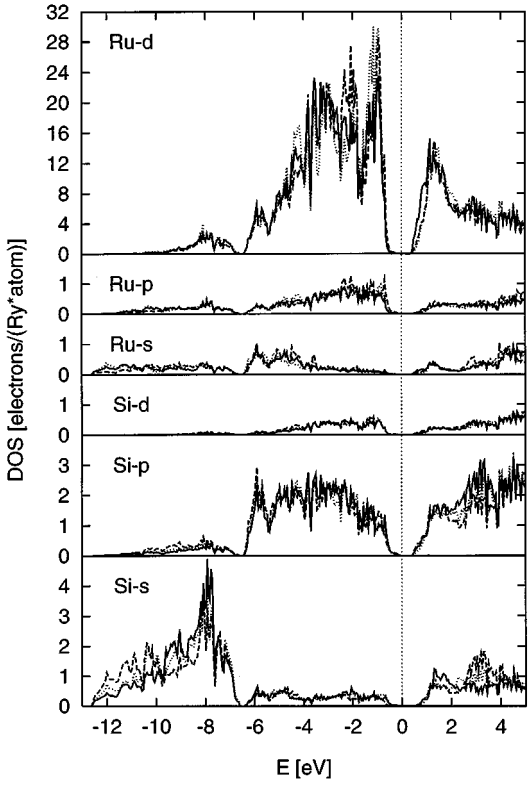

FIG. 6. Local, muffin-tin projected density-of-states of Ru (three top panels) and Si (three bottom panels), decomposed into angular momentum contributions *s* (3rd and 6th panel), *p* (2nd and 5th panel) and *d* (1st and 4th panel). Each panel contains the LDOS of the 3 inequivalent types of Ru(1), Si(1) (short dashed line), Ru(2), Si(2) (long dashed line), and Ru(3), Si(3) (full line) atoms. The LDOS are expressed in units of electrons/Rydberg per atom. Fermi energy is indicated by a vertical dotted line at $E=0$ eV.

This form of increase, which is consistent with the formation of nearly free-electron-like bands in Fig. 5, is due to the Si-Si s-s hybridization (see bottom panel of Fig. 6). This square-root-like behavior comes to an end at the -7 eV gap. Band-structure calculations of the DOS for the hypothetical Si in a TM-silicide lattice without metal atoms[45] do not show this gap nor a pronounced minimum. Thus it is certainly produced by the inclusion of the metal atoms. This gap resembles the split-off s bands found about 9 eV below E_F for III-V semiconductors in the zinc-blende structure, absent for the conventional group-IV semiconductors in the diamond structure. The gap comes from the covalent hybridization between the Si s states with the Ru d states, which is derived from the large contribution of Ru d electrons in this energy regime (first panel of Fig. 6). The formation of the gap depends very subtly on the strength of the hybridization between Si s and Ru d electrons, and thus on the Si and Ru concentrations. For the TM disilicides, the Si-Ru interaction leads to a dip in the DOS, but no gap was observed. On the other hand a gap is found for TM-rich silicides such as Mo_3Si or Mo_5Si_3.[20] Thus, as already discussed for the Si-Ru p-d interaction, Ru_2Si_3 shows bonding properties of transition-metal-rich silicides and the TM disilicides.

Summarizing this part of the work, the hybridization in Ru_2Si_3 leads to the distribution of states shown in terms of the LPDOS in Figs. 5 and 6. The bonding properties are rather complex. In particular, one must consider a mixture of Si-Si, Ru-Si, and Ru-Ru interactions. Putting our information together, we can say that the dominant contributions arise from the Si-Si s-s, Si-Ru s-d, Ru-Ru d-d, and Si-Ru p-d hybridizations. The Si-Si s-s interaction is responsible for the nearly free-electron-like bands, determining in particular the bottom of the valence bands. They are split off due to the Si-Ru s-d hybridization from the main part of the valence bands. The main part of the valence-bands is determined by the Ru-Ru d-d hybridization, which forms bonding and antibonding states. These Ru d-d hybrids interact covalently with the Si p states, forming bonding and antibonding states which are separated by a hybridization gap, in which the Fermi energy is positioned. Some of the d states are hybridized in form of p-d hybrids above the Fermi energy and to the bottom of the actual d-bands. This results effectively in a broad Si-Ru p-d valence-conduction energy-band regime with the largest Si p LPDOS at the extremities of the Si-Ru p-d energy region. The band gap appears just at the edge of the plain Ru-Ru d-d energy just before the energy region is dominated by the Si p bands. We speculate that this might be one reason why a Rh-chimney-ladder compound was never found. Compared to the TM disilicides the Ru sesquisilicide has a lower Si concentration; thus the Ru hybridization has a stronger impact on the Si s and Si p states showing signs of TM-rich silicides, such as the split-off Si s states and the parabolic LPDOS of the Si p states. The Ru s, Ru p, and Si d states seem not to be of much importance for the electronic structure and stability of the compound, with the exception that Ru p electrons make some contributions worth mentioning at the top of the valence bands.

C. Remarks on the width of the gap

According to these results, Ru_2Si_3 is a semiconductor with a gap of about 0.42 eV width. We have also performed band-structure calculations with a reduced basis set for the crystallographic data given by Israiloff and Völlenkle.[37] The lattice parameters given there differ from Table I by 0.2% at a maximum, whereas the internal positions of the atoms can differ as far as 0.12 a.u. We find that the size of the gap varies substantially with respect to these differences in the structural parameters (see Table III). This holds true for both, the FLAPW and a linear-muffin-tin-orbital (LMTO) atomic-sphere approximation[43] calculation, we performed as a cross-check of our results. Furthermore, calculations for a mixed set of crystallographic data consisting of lattice parameters from Israiloff and Völlenkle[37] and internal parameters given by Poutcharovsky and Parthé[36] reveal that the band-gap width is mainly influenced by the choice of the internal parameters.

TABLE III. Dependence of the gap width on the crystallographic parameters used in the calculations. FLAPW (1) refers to a calculation with 55 LAPW's per atom and nine **k** points. In FLAPW 2, 75 LAPW's and 15 **k** points were used.

	Gap width (eV)		
Crystallographic data	LMTO	FLAPW (1)	FLAPW (2)
Ref. 36	0.493	0.427	0.418
Ref. 37	0.581	0.496	
mixed set	0.518	0.440	

Although no optical nor spectroscopic data exist, there is unequivocal experimental evidence[25,26,28] that Ru_2Si_3 is a semiconductor. A band gap of 0.7 eV was reported from high-temperature resistivity experiments around 1000 °C (Ref. 25) and the room-temperature Hall-effect measurements[26] lead to positive carriers with a concentration $n=1.0\times10^{18}$ cm^{-3} and a mobility of $\mu=3.5$ cm^2/V s. Similar results were obtained in Ref. 28.

In the past, ab initio calculations of the electronic structure of silicides particularly carried out by methods which are free of any shape approximation for the charge or potential, such as by FLAPW,[8,9,14,19,33] full potential LMTO,[17,20] or pseudopotential methods[15,21] have described the electronic structure, the band topology and the size of the band-gap quite reliably. The size of the band gap was described much better than for the conventional group-IV or the III-IV semiconductors. It was speculated that the many-body self-energy

TABLE IV. The effective masses along the principle axes of the energy surface for electron and hole states at the Γ point (in units of the free-electron mass) in the vicinity of the band gap.

Band no.	Energy (eV)	M_{xx}	M_{yy}	M_{zz}
109	−0.684	4.586	0.774	0.448
110	−0.610	1.948	1.060	0.308
111	−0.518	−11.726	1.274	0.370
112	0.000	0.468	0.154	0.454
			gap	
113	0.418	3.280	2.852	0.608
114	0.507	4.264	1.054	0.154
115	0.745	10.202	3.984	2.424
116	0.890	−0.434	19.356	−31.426

corrections given by Godby, Schlüter, and Sham,[46] which is large for group-IV or -III-V semiconductors due to the different symmetry of the valence-band (s) states and the conduction-band (p) states, is expected to remain small for the TM silicides, because the states on both sides of the gap are determined largely by states of the same symmetries (typically d symmetry). For Ru_2Si_3 we found a gap which also consists of states with different (p and d) symmetries and, in fact, when we compare our results with experimental data, we have an intermediate situation, where the calculated gap width is smaller than the experimental one, but the error is not in the range typical for DFT results for s-p semiconductors. However, one has to be careful in interpreting our results since—as we have shown—these depend substantially on the exact structural parameters used in the calculation. Mattheiss[8] showed for $CrSi_2$ that the band dispersion of the states around the band gap is particularly sensitive to the Si-atom positions, which determines the TM-Si coordination geometry. Moving the Si position by 6%, the band dispersion of $CrSi_2$ is modified by 0.1 eV. For Ru_2Si_3 this modification could be even larger, since the $4d$ wave function of Ru is more extensive than the $3d$ one of Cr.

D. Effective masses

In order to provide a link between band-structure and transport properties, we calculated the effective mass tensor for valence-band (hole) states and conduction-band (electron) states at the Γ point in the vicinity of the energy gap. Besides the size of the band gap, the effective masses m_1, m_2, and m_3 along the principal axes of the ellipsoidal energy surface are additional important band-structure contributions which determine a possible use of this material in the semiconductor technology. They contribute in terms of the density-of-states effective masses, $(m_1 m_2 m_3)^{1/3}$, to the intrinsic carrier density, and are in terms of the conductivity effective masses, $3(1/m_1+1/m_2+1/m_3)^{-1}$, the band-structure contribution to the carrier mobility. The principle axes have been determined to be along the axes of the reciprocal-lattice vectors, the k_x, k_y, and k_z axes of the orthorhombic Brillouin zone ($m_1=m_{xx}$ and so on). A three-point polynomial fit was used to determine the principal axes, and a five-point polynomial fit was employed to calculate the appropriate second derivatives. A much larger number of basis functions for the electron wave functions was necessary to obtain well-converged results, summarized in Table IV.

From the previously investigated masses of electron and hole states for $CrSi_2$, $MoSi_2$, and WSi_2,[8,48] one knows that the effective masses of states dominated by d character are in the order of the free-electron mass. This seems to be a generic value for masses for states dominated by d character. This is also true for the effective masses we have calculated for Ru_2Si_3. However, Ru_2Si_3 exhibits one exception. The valence bands of the highest occupied state shows a strong dispersion due to the overlap of delocalized Si p states and the corresponding hole masses are about one order of magnitude smaller than the values typical for silicides. They are close to values known for silicon.

V. SUMMARY

In summary we calculated the electronic band structure of the low-temperature phase ($Pbcn$) of the Nowotny chimney-ladder silicide Ru_2Si_3. We find that the electronic structure of this silicide follows the generic trend of silicides with 14 valence electrons per transition-metal atom: low-lying Si s states, Si p–Ru d bands which are separated by a Si p–Ru d covalent hybridization gap, and a Fermi energy which is located in this gap. The gap is direct, and the valence-band maximum and the conduction-band minimum are located at the Γ point in the orthorhombic Brillouin zone. The band gap calculated is about 0.45 eV. The valence-band maximum is predominantly of Si p character and the conduction-band minimum is predominantly of Ru d character. This change of the character of the states by $\Delta l=1$ across the direct gap suggests that Ru_2Si_3 has interesting optical properties, although the strength of the dipole-allowed transition has not yet been calculated, and is left for future investigations. The effective masses of the bands in the vicinity of the gap are in the order of the free-electron mass typical of d states. The band of the highest occupied state, however, exhibits a strong dispersion due to delocalized p states, and the effective mass is therefore already as small as the ones of silicon, suggesting promising transport properties. From the well-known deficiency of the DFT to provide the exact value of the energy gap and the experiences gained in the past decade on group-IV semiconductors and -III-V semiconductors we do not expect any significant change of the band dispersion, but that the true band gap can differ from the calculated one by as much as a factor of 2. We found that structural changes in particular those involving the Ru-Si bond may have a sizable influence on the band gap. Thus, a total theoretical structural optimization of the orthorhombic phase including all atom positions is desirable, and is left for further work. We found further that the complete separation of the Si s states from the Si-Ru p-d hybridization region and the LPDOS of the Si p states show many similarities to the low-symmetry TM-rich silicides. For the isotypical Nowotny chimney-ladder silicides Ru_2Ge_3, Os_2Si_3, and Os_2Ge_3, we expect the same band topology as for Ru_2Si_3, but with modifications for the size of the band gap and small rearrangements of the dispersion of the bands all of which are important for the potential application of these silicides. Much could be learned from additional optical or spectroscopic experiments.

ACKNOWLEDGMENTS

We thank Dr. S. Mantl for bringing the subject to our attention, and for the fruitful discussions during the course of this work. We also gratefully acknowledge the helpful comments of R. Podloucky on our work. G. B. would like to thank the Human Capital and Mobility Program ''Ab initio (from electronic structure) calculation of complex processes in materials'' (Contract: ERBCHRXCT930369) of the European Union. This work was also supported by the Center of Excellence for Computational Materials Science (CMS), Vienna. The computations were performed at the Vienna University computing center and the Forschungszentrum Jülich. The LMTO calculations were carried out with the program LMTOPACK coded by T. Oguchi.

*Permanent address: Institute für Physikalische Chemie, Universität Wien, A-1090 Wien, Austria.
†Electronic address: s.bluegel@kfa-juelich.de

[1] S. P. Murarka and M. C. Peckerar, in *Electronic Materials, Science and Technology*, edited by J. Streichen (Academic, Boston, 1989), p. 267.
[2] S. P. Murarka, *Silicides for VLSI Applications* (Academic, New York, 1983).
[3] J. C. Hensel, A. F. Levi, R. T. Tung, and J. M. Gibson, Appl. Phys. Lett. **47**, 151 (1985).
[4] G. V. Samsonov and I. M. Vinitskii, *Handbook of Refractory Compounds* (IFI/Plenum, New York, 1980).
[5] G. V. Samsonov, *Handbook of High-Temperature Materials* (Plenum, New York, 1964), Vol. 2.
[6] M. C. Bost and J. E. Mahan, J. Vac. Sci. Technol. B **4**, 1336 (1986).
[7] D. Shinoda, S. Asanabe, and Y. Sasaki, J. Phys. Soc. Jpn. **19**, 269 (1964).
[8] L. F. Mattheiss, Phys. Rev. B **43**, 1863 (1991).
[9] L. F. Mattheiss, Phys. Rev. B **43**, 12 549 (1991).
[10] M. P. C. M. Krijn and R. Eppenga, Phys. Rev. B **44**, 9042 (1991).
[11] S. V. Halilov and E. T. Kulatov, Semicond. Sci. Technol. **7**, 368, (1992).
[12] V. Bellani *et al.*, Phys. Rev. B **46**, 9380 (1992).
[13] A. B. Filonov *et al.*, Phys. Status Solidi B **186**, 209 (1994).
[14] L. F. Mattheiss and J. C. Hensel, Phys. Rev. B **39**, 7754 (1989).
[15] B. K. Bhattacharyya, D. M. Bylander, and L. Kleinman, Phys. Rev. B **32**, 7973 (1985).
[16] S.-P. Tang and K.-M. Zhang, J. Phys. C **21**, 1469 (1988).
[17] M. Alouani, R. C. Albers, and M. Methfessel, Phys. Rev. B **43**, 6500 (1991).
[18] A. E. Carlsson and P. J. Meschter, J. Mater. Res. **6**, 1512 (1991).
[19] L. F. Mattheiss, Phys. Rev. B **45**, 3252 (1992).
[20] A. K. McMahan, J. E. Klepeis, M. van Schilfgaarde, and M. Methfessel, Phys. Rev. B **50**, 10 742 (1994).
[21] B. K. Bhattacharyya, D. M. Bylander, and L. Kleinman, Phys. Rev. B **31**, 2049 (1985); **31**, 5462 (1985).
[22] F. M. d'Heurle, C. Petersson, and M. Y. Tsai, J. Appl. Phys. **51**, 5976 (1980).
[23] W. T. Lin and L. J. Chen, J. Appl. Phys. **59**, 1518 (1986).
[24] W. T. Lin and L. J. Chen, J. Appl. Phys. **59**, 3481 (1986).
[25] C. P. Susz, J. Muller, K. Yvon, and E. Parthé, J. Less-Common Metals **71**, P1 (1980).
[26] U. Gottlieb, O. Laborde, A. Rouault, and R. Madar, Appl. Surf. Sci. **73**, 243 (1993).
[27] Y. S. Chang and J. J. Chu, Mater. Lett. **5**, 67 (1987).
[28] C. B. Vining and C. E. Allevato, in *Proceedings of the 10th International Conference on Thermoelectrics, Cardiff, Wales, UK, 10-12 September 1991*, edited by D. M. Rowe (Babrow, Cardiff, 1991), p. 167.
[29] H. Nowotny, in *The Chemistry of Extended Defects in Nonmetallic Solids*, edited L. R. Eyring and M. O'Keefe (North-Holland, Amsterdam, 1970), p. 223.
[30] E. Parthé, in *Developments in the Structural Chemistry of Alloy Phases* (Plenum, New York, 1966), 55.
[31] W. B. Pearson, Acta Crystallogr. B **26**, 1044 (1970).
[32] W. Jeitschko and E. Parthé, Acta Crystallogr. **22**, 417 (1967).
[33] S. Eisebitt, J.-E. Rubensson, M. Nicodemus, T. Böske, S. Blügel, W. Eberhardt, K. Radermacher, S. Mantl, and G. Bihlmayer, Phys. Rev. B **50**, 18 330 (1994).
[34] R. Eppenga, J. Appl. Phys. **68**, 3027 (1990).
[35] P. Pécheur and G. Toussaint, Phys. Lett. A **160**, 193 (1991).
[36] D. J. Poutcharovsky and E. Parthé, Acta Crystallogr. B **30**, 2692 (1974).
[37] P. Israiloff and H. Völlenkle, Monatsh. Chem. **105**, 1313 (1974).
[38] *Pearson's Handbook of Crystallographic Data for Intermetallic Phases*, edited by P. Villars and L. D. Calvert (American Society for Metals, Metals Park, 1985), Vol. 1.
[39] D. J. Poutcharovsky, K. Yvon, and E. Parthé, J. Less-Common Metals **40**, 139 (1975).
[40] L. Hedin and B. I. Lundqvist, J. Phys. C **4**, 2064 (1971).
[41] E. Wimmer, H. Krakauer, M. Weinert, and A. J. Freeman, Phys. Rev. B **24**, 864 (1981), H. F. Jansen and A. J. Freeman, Phys. Rev. B **30**, 561 (1984).
[42] O. Jepson and O. K. Andersen, Solid State Commun. **9**, 1763 (1971); G. Lehmann and M. Taut, Phys. Status Solidi B **54**, 469 (1972).
[43] O. K. Andersen, Phys. Rev. B **12**, 3060 (1975); H. L. Skriver, *The LMTO Method* (Springer Verlag, Heidelberg, 1983).
[44] A. P. Cracknell, B. L. Davies, S. C. Miller, and W. F. Love, *Kronecker Product Tables* (Plenum, New York 1979), Vol. I.
[45] P. J. W. Weijs, M. T. Czyzyk, J. C. Fuggle, W. Speier, D. D. Sarma, and K. H. J. Buschow, Z. Phys. B **78**, 423 (1990).
[46] R. W. Godby, M. Schlüter, and L. J. Sham, Phys. Rev. Lett **56**, 2415 (1986); Phys. Rev. B **36**, 6497 (1987).
[47] C. J. Bradley and A. P. Cracknell, *The Mathematical Theory of Symmetry in Solids* (Oxford University Press, Oxford, 1972).
[48] A. B. Filonov, I. E. Tralle, N. N. Dorozhkin, D. B. Migas, V. L. Shaposhnikov, G. V. Petrov, V. M. Anishchik, and V. E. Borinsenko, Phys. Status Solidi B **186**, 209 (1994).